

Resilience of Bayesian Layer-Wise Explanations under Adversarial Attacks

Ginevra Carbone¹

Guido Sanguinetti^{2,3}

Luca Bortolussi^{1,4}

¹Dept. of Mathematics and Geosciences, University of Trieste, Trieste, Italy

²SISSA, Trieste, Italy

³School of Informatics, University of Edinburgh, Edinburgh, United Kingdom

⁴Modeling and Simulation Group, Saarland University, Saarland, Germany

Abstract

We consider the problem of the stability of saliency-based explanations of Neural Network predictions under adversarial attacks in a classification task. We empirically show that, for deterministic Neural Networks, saliency interpretations are remarkably brittle *even when the attacks fail*, i.e. for attacks that do not change the classification label. By leveraging recent results, we provide a theoretical explanation of this result in terms of the geometry of adversarial attacks. Based on these theoretical considerations, we suggest and demonstrate empirically that saliency explanations provided by Bayesian Neural Networks are considerably more stable under adversarial perturbations. Our results not only confirm that Bayesian Neural Networks are more robust to adversarial attacks, but also demonstrate that Bayesian methods have the potential to provide more stable and interpretable assessments of Neural Network predictions.

1 INTRODUCTION

Deep Neural Networks (DNNs) are the core engine of the modern AI revolution. Their universal approximation capabilities, coupled with advances in hardware and training algorithm, have resulted in remarkably strong predictive performance on a variety of applications, from computer vision to natural language to bioinformatics.

While the story of DNNs is indubitably one of success, it is tempered with a number of potentially very serious drawbacks which are somehow the natural flip side of dealing with extremely flexible and complex models. The first such drawback is the black box nature of DNNs: their expressivity and training on large data sets empirically results in very strong predictive power, but in general it does not provide

any intuition about the possible explanations underlying the decisions. The opaqueness of DNNs decisions is a major hurdle towards their usage in scientific applications, where frequently explanations for decisions are even more important than accuracy. It is even more problematic in many societal applications, where several countries mandate by law the explainability of any algorithmic decision in a variety of contexts.

A second major drawback of DNN predictions is their vulnerability to adversarial attacks: empirically, it has been observed in many applications that well chosen infinitesimal changes in inputs can produce catastrophic changes in output [Goodfellow et al., 2015], leading to paradoxical classifications and a clear problem in any application to safety critical systems. Such brittleness appears to be intimately related to the geometry of the data itself [Carbone et al., 2020], and is therefore likely to be an intrinsic feature of standard DNN predictions.

In this paper, we argue theoretically and empirically¹ that these two problems are interlinked, and that therefore solutions that ameliorate resilience against adversarial attacks will also lead to more stable and reliable interpretations. We work within the framework of (pixel-wise) saliency explanations, which attempt to interpret post-hoc DNN decisions by apportioning a relevance score to each input feature for each data point. Specifically, we use the popular Layer-wise Relevance Propagation (LRP) [Bach et al., 2015], a method to assess the contribution of each pixel to the final classification score which backpropagates the prediction in the neural network until it reaches the input, using a set of suitable propagation rules. LRP saliency interpretations are well known to be unstable under perturbations of the inputs [Ghorbani et al., 2019, Kindermans et al., 2019, Alvarez-Melis and Jaakkola, 2018, Zhang et al., 2020]; recently, Bykov et al. [2020] suggested that a Bayesian treatment might ameliorate these stability problems.

¹Code is available at <https://github.com/ginevracoal/BayesianRelevance>

Here, we consider the stability of saliency interpretations under targeted adversarial attacks that aim to change the classification under perturbations of the input. We introduce a novel notion of LRP robustness under adversarial attacks. To our surprise, we found that the LRP robustness of deterministic DNN predictions was remarkably low even when the adversarial attack failed to change the overall classification of the data point, i.e., LRP interpretations appear to be *less robust* than actual classifications. We analyse theoretically the geometry of LRP robustness in a suitably defined large-data limit [Carbone et al., 2020, Rotskoff and Vanden-Eijnden, 2018, Du et al., 2019, Mei et al., 2018], and argue that the observed lack of robustness might be imputable to large gradients of the prediction function in directions orthogonal to the data manifold. Leveraging recent results from Carbone et al. [2020], we argue that a Bayesian training of the DNNs should lead to an improved LRP robustness, as well as stronger robustness to adversarial attacks. We empirically validate our hypothesis on the popular MNIST and Fashion MNIST benchmarks.

The main contributions of this paper are:

1. the definition of a novel metric of robustness of interpretations of DNN results (Sec. 3.1);
2. a theoretical analysis of the effects of adversarial attacks on prediction interpretations, and of the improvements offered by a Bayesian treatment (Sec. 3.2);
3. an empirical study showing that indeed Bayesian training and prediction leads to more robust interpretations of classifications (Sec. 4).

2 BACKGROUND

2.1 LAYER-WISE RELEVANCE PROPAGATION

Let $f : \mathbb{R}^d \rightarrow [0, 1]$ be a single-class image classifier, where $f(x, w)$ is the probability that an image $x \in \mathbb{R}^d$ belongs to the class of interest and w is the set of learnable weights. Without loss of generality, this concept can be extended to multi-class classifiers or to non probabilistic outputs. The idea of pixel-wise decomposition of a given image x is to understand how its pixels contribute to the prediction $f(x, w)$. In particular, LRP associates with each pixel p a relevance score $R(x_p, w)$, which is positive when the pixel contributes positively to the classification, negative when it contributes negatively to the classification and zero when it has no impact on the classification. All the relevance scores for a given image x can be stored in a heatmap $R(x, w) = \{R(x_p, w)\}_p$, whose values quantitatively explain not only whether pixels contribute to the decision, but also by which extent. By leveraging suitable propagation rules, one can ensure that relevance heatmap catch saliency features. For this purpose, the heatmap should be *conservative*, i.e. the sum of the assigned relevances should correspond to the

total relevance detected by the model

$$f(x, w) = \sum_p R(x_p, w).$$

Several propagation rules satisfy the conservative property, each of them leading to different relevance measures. A practical example of propagation rule is the *Epsilon rule* (ε -LRP) [Montavon et al., 2019]. Let a_j be a neuron activation computed at the j -th layer during the forward pass. Let w_{jk} be the weight connecting a_j to a subsequent neuron a_k , w_{0k} be the bias weight and $a_0 = 1$. At each step of backpropagation LRP computes the relevance score R_j of the j -th activation a_j , by backpropagating the relevance scores of all neurons in the subsequent layer. The resulting ε -LRP score for a chosen $\varepsilon > 0$ amounts to

$$R_j = \sum_k \frac{a_j w_{jk}}{\varepsilon + \sum_{0,j} a_j w_{jk}} R_k. \quad (1)$$

Bach et al. [2015] also presented LRP using a functional approach, i.e. independently of the network's topology. Then, Montavon et al. [2017] used *deep Taylor decomposition* to interpret rule-based approaches under the functional setting. Their method builds on the standard first-order Taylor expansion of a non-linear classifier at a chosen *root point* \tilde{x} , such that $f(\tilde{x}) = 0$,

$$\begin{aligned} f(x) &= f(\tilde{x}) + \nabla_x f(\tilde{x}) \cdot (x - \tilde{x}) + \gamma \\ &= \sum_p \frac{\partial f}{\partial x_p} \Big|_{x=\tilde{x}} \cdot (x_p - \tilde{x}_p) + \gamma, \end{aligned} \quad (2)$$

where γ denotes higher-order terms. The root point \tilde{x} represents a neutral image which is similar to x , but does not influence classification, i.e. whose relevance is everywhere null. The nearest root point to the original image x can be obtained by solving an iterative minimization problem [Montavon et al., 2017].

2.2 ADVERSARIAL ATTACKS

Adversarial attacks are small perturbations of input data that lead to large changes in output (in the classification case, changes in predicted label) Goodfellow et al. [2015]. Broadly speaking, most attack strategies utilise information on the DNN loss function to detect an optimal perturbation direction, either through explicit knowledge of the loss function (*white box attacks*) or via querying the DNN (*black box attacks*, generally weaker than their white box counterpart).

White box attacks generally utilize gradient information on the loss function to determine the attack direction. One of the best known gradient-based attacks is the Fast Gradient Sign Method (FGSM) [Goodfellow et al., 2015], a one-step untargeted attack (i.e., an attack strategy which is independent of the class of the attacked point). For a given network $f(\cdot, w)$ it crafts a perturbation in the direction of the greatest

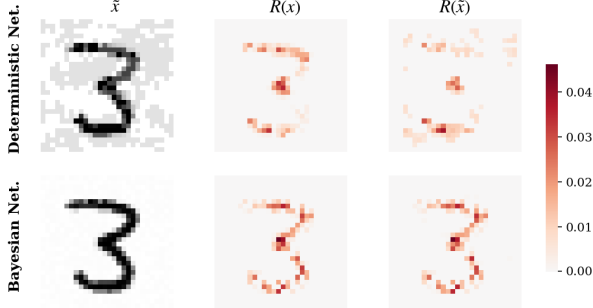


Figure 1: LRP heatmaps of an image x (second column) and an FGSM adversarial perturbation \tilde{x} (third column) which fails on a deterministic network and a Bayesian network. The two models have the same architecture (Tab. 2) and are both trained on the MNIST dataset. Explanations are computed on the pre-softmax layer, i.e. layer $\text{idx} = 5$ from Tab. 2. Bayesian LRP is computed using 100 posterior samples. For each heatmap we only show the 100 most relevant pixels. The LRP robustness amounts to 0.58 in the deterministic case and to 0.93 in the Bayesian case.

loss w.r.t. the input

$$\tilde{x} = x + \delta \operatorname{sgn} \nabla_x L(x, w),$$

where L is the training loss and δ is the perturbation magnitude (*strength* of the attack). An iterative, improved version of FGSM is Projected Gradient Descent (PGD) Kurakin et al. [2016]. PGD starts from a random perturbation in an ϵ - L_∞ ball around the input sample. At each step, it performs FSGM with a smaller step size, $\alpha < \epsilon$, and projects the adversary back in the ϵ - L_∞ ball

$$x_{t+1} = \operatorname{Proj}\{x_t + \alpha \cdot \operatorname{sgn} \nabla_x L(x_t, w)\}.$$

The size of the resulting perturbation is smaller than ϵ .

The evaluation of adversarial attacks can be either qualitative or quantitative. In the qualitative case, one simply observes whether an attack strategy with a certain strength is successful in switching the classification label of the given data point; in general, the evaluation then reports the fraction of successful attacks on the whole data set. A quantitative metric to evaluate network performances against adversarial attacks is provided by the notion of *softmax robustness* [Carbone et al., 2020], which computes the softmax difference between original and adversarial predictions

$$1 - \|f(x) - f(\tilde{x})\|_\infty. \quad (3)$$

and is a number between zero (maximal fragility) and one (complete robustness) for every data point.

2.3 BAYESIAN NEURAL NETWORKS

Bayesian models capture the inherent uncertainty intrinsic in any model by replacing individual models with ensem-

bles weighted by probability laws. In the DNN setup, a Bayesian Neural Network (BNN) consists of an ensemble of DNNs whose weights are drawn from the posterior measure $p(w|D)$, where D denotes the available training data. To compute the posterior measure, one needs to first define a prior distribution $p(w)$ on the network’s weights w ; by Bayes’ theorem, the posterior is then obtained by combining the prior and the likelihood $p(w|D) \propto p(D|w)p(w)$, where the likelihood term $p(D|w)$ quantifies the fit of the network with weights w to the available training data. Exact computation of the posterior distribution $p(w|D)$ is in general infeasible, thus one needs to resort to approximate inference methods for training Bayesian NNs, namely Hamiltonian Monte Carlo (HMC) [Neal et al., 2011] and Variational Inference (VI) [Wainwright and Jordan, 2008].

Once the posterior distribution has been computed, BNNs produce predictions through the *posterior predictive distribution*

$$\begin{aligned} p(f(x)|D) &= \int d\mathbf{w} p(f(x)|\mathbf{w})p(\mathbf{w}|D) \\ &\simeq \sum_{\mathbf{w}_j \sim p(\mathbf{w}|D)} p(f(x)|\mathbf{w}_j) \end{aligned} \quad (4)$$

where $f(x)$ is the output value at a new point x , and the equality represents the celebrated *Bayesian model averaging* procedure.

In the BNN setting, adversarial attacks are crafted against the posterior predictive distribution $p(f(x)|D)$. For example, FGSM attack on an ensemble of N networks $f(\cdot, w_i)$ with weights drawn from $p(w|D)$ becomes

$$\begin{aligned} \tilde{x} &= x + \delta \operatorname{sgn} \left(\mathbb{E}_{p(w|D)} [\nabla_x L(x, w)] \right) \\ &\simeq x + \delta \operatorname{sgn} \sum_{i=1}^N \nabla_x L(x, w_i) \quad w_i \sim p(w|D). \end{aligned}$$

In a similar way, it is possible to introduce a concept of *Bayesian explanations* for BNN predictions. As is clear from the definition(s) of LRP in Section 2.1, the relevance score assigned to an input feature depends on the neural network weights. Therefore, in the Bayesian setting, the relevance becomes a random variable; we define as a Bayesian explanation the expected relevance of a feature under the posterior distribution of the weights.

Recent research shows that Bayesian neural networks are adversarially robust to gradient-based attacks in the over-parametrised and infinite data limit [Carbone et al., 2020, Rotskoff and Vanden-Eijnden, 2018]. It is therefore of interest to investigate whether such robustness also extends to the learned explanations. To do so, we compare the explanations of deterministic NNs to that of Bayesian NNs against such attacks. Fig. 1 shows an example of failed FGSM attack for a deterministic network and a Bayesian network with the same architecture. Despite the fact that the attack did

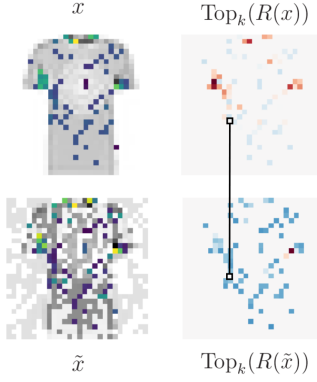


Figure 2: Top₂₀₀ pixels in an image x from Fashion MNIST dataset and an FGSM adversarial perturbation \tilde{x} .

not manage to change the overall classification, we can see immediately a large difference between the deterministic LRP explanation of the original image, $R(x)$, and of the adversarial image, $R(\tilde{x})$ (top row). On the other hand, in the Bayesian case (bottom row), the saliency maps before and after the attack are essentially identical. In the next sections, we will provide both a theoretical explanation of this phenomenon, and systematically substantiate empirically the robustness of Bayesian explanations to adversarial attacks.

3 METHODOLOGY

3.1 LRP ROBUSTNESS

We define the k -LRP robustness of relevance heatmaps to adversarial attacks and use this measure to assess how adversarial perturbations affect the explanations.

Definition 3.1. Let x be an image with relevance heatmap $R(x, w)$ and \tilde{x} an adversarial perturbation with relevance heatmap $R(\tilde{x}, w)$. Let $\text{Top}_k(R)$ denote the set of k most relevant pixel indexes in a heatmap R , where $P \in \mathbb{N}$ is the total number of pixels in x and $k \leq P$. The k -LRP robustness of x w.r.t. the attack \tilde{x} is

$$k\text{-LRP}_\rho(x, \tilde{x}, w) := \frac{|\text{Top}_k(R(x, w)) \cap \text{Top}_k(R(\tilde{x}, w))|}{k}. \quad (5)$$

In other words, k -LRP _{ρ} (x, \tilde{x}, w) is the fraction of common k most relevant pixels for x and \tilde{x} . Fig. 2 gives an intuition of this computation. Notice that the LRP robustness of a point depends only implicitly on the strength of the attack through the attacked point \tilde{x} .

Inner layers explanations We analyse the behaviour of LRP representations in the internal layers of the network, thus we also extend the computation of LRP heatmaps to any feature representation of the input x at a learnable layer $l \in \mathbb{N}$. We denote it by $R(x, w, l)$, where $l \leq L$ and L is

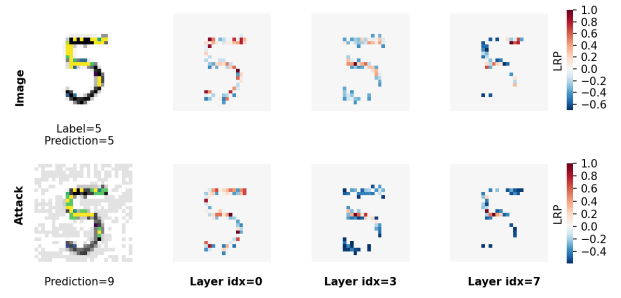


Figure 3: LRP heatmaps of an image x and an FGSM adversarial perturbation \tilde{x} . Explanations are computed w.r.t. the learnable layers of a deterministic network trained on the MNIST dataset. For each layer, we only show the 100 most relevant pixels for both the original image and its adversarial counterpart, i.e. the ones selected for the computation of $100\text{-LRP}_\rho(x, \tilde{x}, w, l)$ from Eq. (5), where $l \in [0, 3, 7]$.

the maximum number of layers available in the architecture. The corresponding LRP robustness will be denoted by $k\text{-LRP}_\rho(x, \tilde{x}, w, l)$. In such case, the robustness does not refer anymore to explanations in the classification phase (pre-softmax layer), but rather to the explanations in the learning phases, hence it gives an idea of the most relevant pixels determining an internal representation. Fig. 3 shows an example of internal LRP heatmaps on a deterministic NN with learnable layers indexed by $l \in [0, 3, 7]$. For illustrative purposes, heatmaps appearing on the same row are normalized in $[-1, 1]$ before selecting the Top_k pixels, since numeric scales are significantly different across the different internal representations.

Bayesian LRP robustness The notion of LRP robustness can be naturally generalised to the Bayesian setting using the concept of Bayesian model averaging introduced in Section 2.3. Hence, the LRP heatmap of a BNN is computed as the average of all the deterministic heatmaps from the ensemble:

$$\mathbb{E}_{p(w|D)} [k\text{-LRP}_\rho(x, \tilde{x}, w, l)].$$

In this regard, we emphasise that Bayesian interpretations are affected by the chosen number of posterior samples drawn from the learned distribution.

3.2 GEOMETRIC MEANING OF ADVERSARIAL INTERPRETATIONS

To better conceptualise the impact of a Bayesian treatment on LRP robustness, it is convenient to consider the thermodynamic limit of infinite data and infinite expressivity of the network, as formalised in Du et al. [2019], Mei et al. [2018], Rotskoff and Vanden-Eijnden [2018]. We refer the reader to Carbone et al. [2020] for a thorough mathematical discussion of the assumptions corresponding to this thermodynamic limit. For the purposes of our discussion, the

main ingredients are the data manifold \mathcal{M}_D , a piecewise smooth submanifold of the input space where the data lie, and the true input/output function $g(x)$, which is assumed to be smooth and hence representable through an infinitely wide DNN. Practically, this limit might be well approximated on large data sets where the networks achieve high accuracy.

In this limit, it was proved in Du et al. [2019], Mei et al. [2018], Rotskoff and Vanden-Eijnden [2018] that the DNN $f(x, w)$ trained via SGD will converge to the true underlying function $g(x)$ over the whole data manifold \mathcal{M}_D . Because the data manifold is assumed to be piecewise smooth, it is possible to define a tangent space to the data manifold almost everywhere, and therefore to define two operators ∇_x^\perp and ∇_x^\parallel which define the gradient along the normal and tangent directions to the data manifold \mathcal{M}_D at a point x of a function defined over the whole input space.

LRP and gradient-based adversarial strategies both share a reliance on gradient information. In the adversarial attacks cases, one evaluates the gradient of the loss function which, by the chain rule is given by

$$\nabla_x L(f, g) = \frac{\delta L(f, g)}{\delta f} \frac{\partial f}{\partial x} \quad (6)$$

In the thermodynamic limit, the DNN function $f(x, w)$ coincides with the true function everywhere on the data manifold, and therefore the tangent gradient of the loss function is identically zero. The normal gradient of the loss, however, is unconstrained by the data, and, particularly in a high dimensional setting, might achieve very high values along certain directions, creating therefore weaknesses that may be exploited by an adversarial attacker. The main result of Carbone et al. [2020] was to show that the orthogonal component of the loss gradient has expectation zero under the posterior weight distribution, therefore showing that BNNs are robust against adversarial attacks.

In the LRP setup, we instead consider gradients of the prediction function, as opposed to the loss, nevertheless the insight remains valid. The tangent components of the gradient of the prediction function $f(x, w)$ will coincide with the gradients of the true function $g(x)$, and therefore represent directions of true sensitivity of the decision function which are correctly recognised as relevant. However, such directions might be confounded or dwarfed by normal gradient components, which create directions of apparent relevance which, by construction, are targeted by gradient-based adversarial attacks.

Because the normal gradient of the loss function (6) is proportional to the normal gradient of the prediction function, the zero-averaging property under the posterior will be inherited by the gradient of the prediction function, so that

$$E_{p(w|D)}[\nabla_x^\perp f(x, w)] = 0.$$

Therefore, BNNs in the thermodynamic limit will only retain relevant directions along the data manifold, which correspond to genuine directions of high relevance.

4 EXPERIMENTAL RESULTS

In this section we corroborate the insights described in Section 3 with an experimental evaluation, comparing empirically the LRP robustness using the popular MNIST [LeCun and Cortes, 2010] and Fashion MNIST [Xiao et al., 2017] benchmark data sets. Both data sets are composed of 60.000 images belonging to ten classes: in the MNIST case, these are hand-written digits, while the Fashion MNIST data set consists of stylized Zalando images of clothing items. While MNIST is considered a relatively trivial data set, with accuracies over 99% being regularly reported, Fashion MNIST is considerably more complex, and the best architectures report accuracies around 95%. We do not experiment on more complex data sets such as CIFAR-10 [Krizhevsky et al.] or ImageNet [Deng et al., 2009], because of the very high computational costs of running Bayesian inference on very deep networks trained on very large data sets².

On both data sets, we train deterministic DNNs and BNNs using both HMC and VI: this allows us to contrast the effect of a locally Gaussian approximation to the posterior against the asymptotically exact (but computationally more expensive) approximation provided by HMC. Because we require high accuracy in order to approximate the asymptotic conditions described in Section 3.2, different architectures were used on the two data sets and between VI and HMC. In all cases, however, the BNN is compared with a DNN with the same architecture, to ensure fairness of the comparisons. Full details of the architectures used are reported in Sec. 6.1 of the Appendix.

Adversarial attacks in our tests are Fast Gradient Sign Method (FGSM) [Goodfellow et al., 2015] and Projected Gradient Descent (PGD) [Kurakin et al., 2016], with a maximum perturbation size of 0.25. We rely on *TorchLRP* library³ for the computation of LRP explanations and set $\epsilon = 0.1$ in the Epsilon rule.

4.1 BAYESIAN INTERPRETATIONS ARE ROBUST AGAINST ATTACKS

Our first significant result is that Bayesian explanations are considerably more robust under attacks than deterministic architectures. For both data sets and both VI and HMC training, LRP robustness scores are significantly higher than their deterministic counterparts. These results are shown

²We do not experiment with scalable Monte Carlo dropout methods Gal and Ghahramani [2016] here since the properties of the posterior approximation they provide are not well understood.

³<https://github.com/fhvilsthoj/TorchLRP>

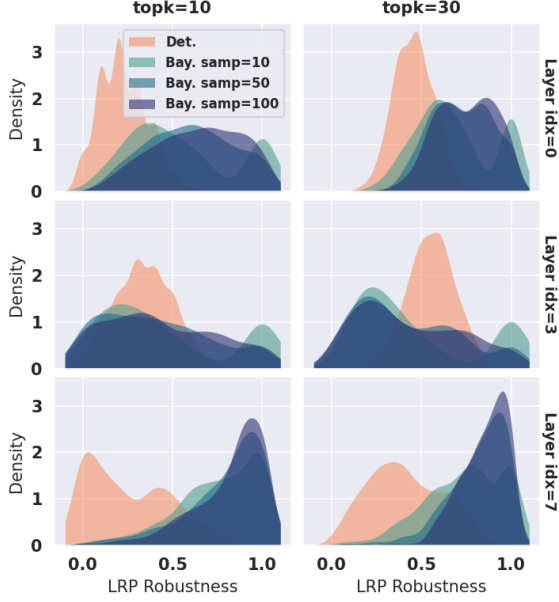


Figure 4: LRP robustness distributions computed on 500 test points from MNIST dataset. Bayesian networks are trained with VI and tested on an increasing number of samples (10, 50, 100). Layer indexes refer to the learnable layers in the architecture (Tab. 1 in the Appendix), which is shared across models.

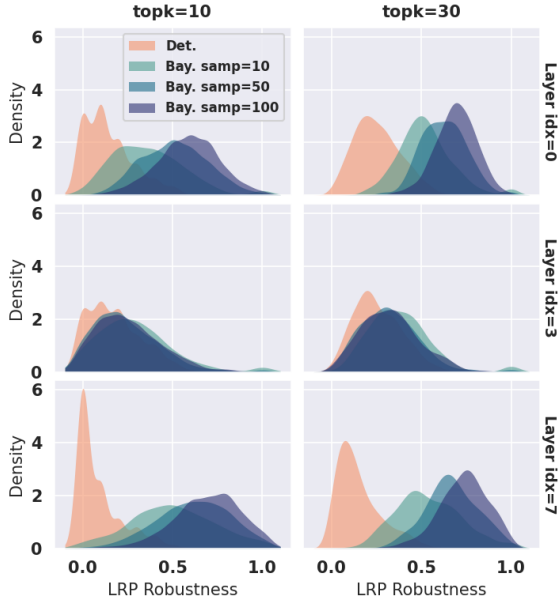


Figure 5: LRP robustness distributions computed on 500 test points from Fashion MNIST dataset. Bayesian networks are trained with VI and tested on an increasing number of samples (10, 50, 100). Layer indexes refer to the learnable layers in the architecture (Tab. 1 in the Appendix), which is shared across models.

for the MNIST data set in Fig. 6 (HMC training) and 4 (VI training), and in Fig. 7 (HMC) and 5 (VI) for Fashion

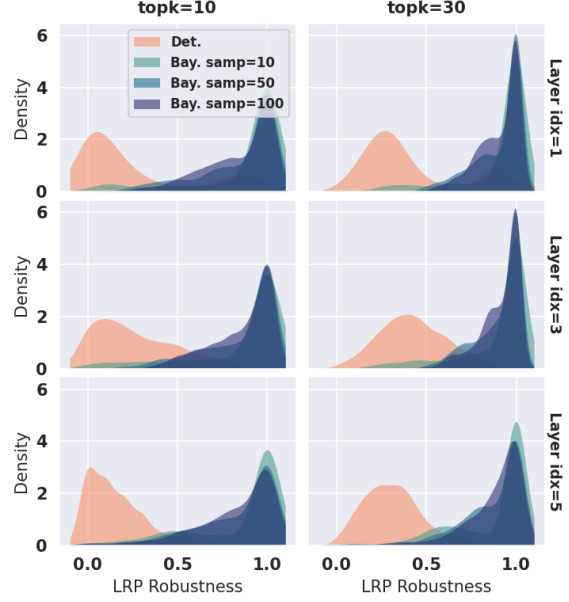


Figure 6: LRP robustness distributions computed on 500 test points from MNIST dataset. Bayesian networks are trained with HMC and tested on an increasing number of samples (10, 50, 100). Layer indexes refer to the learnable layers in the architecture (Tab. 2 in the Appendix), which is shared across models.

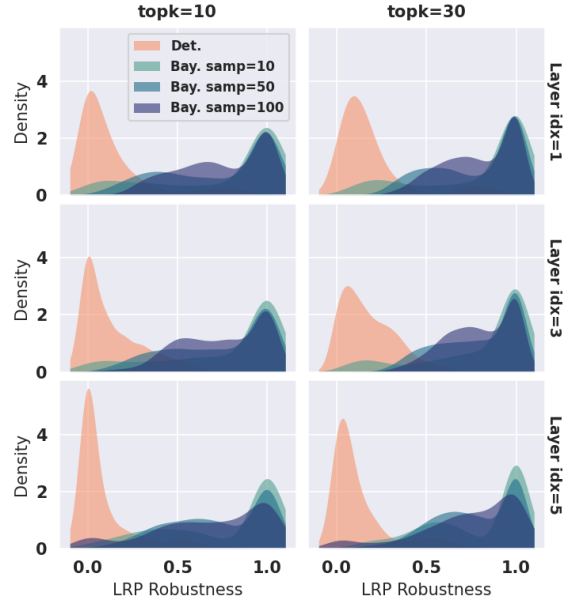


Figure 7: LRP robustness distributions computed on 500 test points from Fashion MNIST dataset. Bayesian networks are trained with HMC and tested on an increasing number of samples (10, 50, 100). Layer indexes refer to the learnable layers in the architecture (Tab. 2 in the Appendix), which is shared across models.

MNIST. The last row of the figures represents the standard LRP (computed from the pre-softmax layer), while the top

row is the initial feature representation (after the first non-linear layer), and the middle row represents the LRP of an internal layer. We tested Bayesian representations using an increasing number of posterior samples, i.e. 10, 50, 100 and two different choices of k , $k = 10$ and $k = 30$ (columns). We attacked 500 randomly selected test images, whose choice is balanced w.r.t. the available classes, and plot the distribution of the resulting LRP scores.

The first notable observation is that in both data sets and with both inference method the Bayesian (pre-softmax) LRP has robustness values very close to one. Interestingly, the behaviour of the LRP in the inner layers appears to be rather different between VI and HMC: while HMC seems stable across all layers, networks trained with VI appear to have a broadening of the LRP distribution in the intermediate layers, suggesting that compensatory changes happen between the early and late layers. Importantly, we see that deterministic DNNs have very low LRP robustness, particularly in the $k = 10$ case: this confirms empirically the conjecture of Section 3.2 that components of the gradient that are normal to the data manifold (and are therefore the ones likely to be changed in an attack) are often major contributors to the relevance in DNN. On the contrary, the Bayesian averaging process greatly reduces the expected relevance of such direction; importantly, we see that this reduction is larger the greater the number of samples, as should be expected.

4.2 BAYESIAN LRP ROBUSTNESS IS CORRELATED WITH SOFTMAX ROBUSTNESS

A simple explanation for the improved LRP robustness of BNNs lies in the fact that BNNs are provably immune to gradient-based attacks [Carbone et al., 2020]. Therefore, one might argue that the stability of the LRP is a trivial byproduct of the stability of the classifications.

To explore this question more in depth, we consider the relationship between the LRP robustness of a test point (stability of the explanation) and its softmax robustness (resilience of the classification against an attack). Fig. 8 and 9 present scatterplots of these two quantities for the models from the previous experiments. An immediate observation is that deterministic explanations are weak against adversarial perturbations even when their softmax robustness (3) is close to 1. Therefore, even in the cases where the classification is unchanged, deterministic saliency heatmaps are fragile. In fact, there are no significant changes in LRP robustness between data points that are vulnerable to attacks and data points that are robust to attacks. Bayesian models, instead, show a strong positive correlation between LRP and softmax robustness, especially as the number of posterior samples increases. While it is immediately evident that Bayesian predictions are robust to adversarial attacks (since most data points have softmax robustness greater than 0.5),

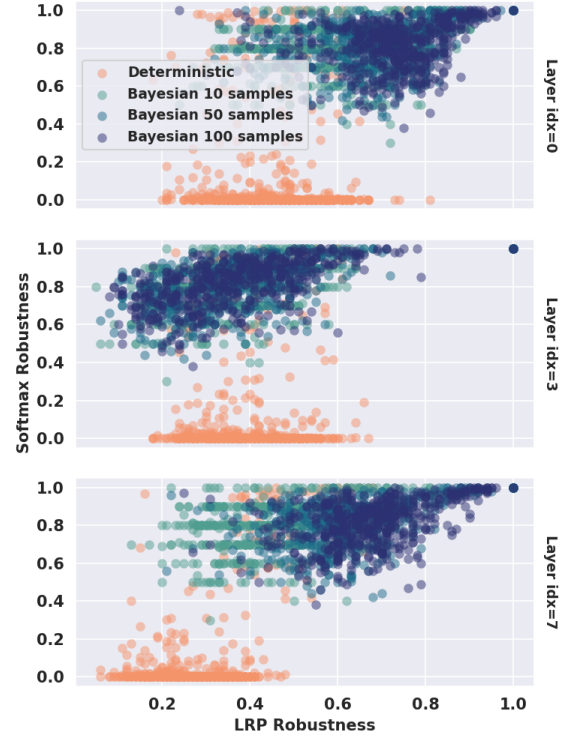


Figure 8: LRP vs Softmax Robustness of deterministic and Bayesian NNs trained on Fashion MNIST dataset. LRP Robustness is computed on the 100 most relevant pixels, i.e. using Top₁₀₀. Bayesian Networks are trained with VI and tested on an increasing number of samples (10, 50, 100). Layer indexes refer to the learnable layers in the architecture (Tab. 1 in the Appendix), which is shared across all models.

it is also clear from this correlation that attacks which are more successful (i.e. lower softmax robustness) also alter more substantially the interpretation of the classification, and are therefore likely to represent genuine directions of change of the true underlying decision function along the data manifold.

5 CONCLUSIONS

Deep neural networks are fundamental to modern AI, yet many of the mathematical structures underlying their success are still poorly understood. Unfortunately, an unavoidable consequence of this situation is that we also lack principled tools to address the weaknesses of deep learning systems.

In this paper, we harness the geometric perspective to adversarial attacks introduced in Carbone et al. [2020] to study the resilience of Layer-wise Relevance Propagation heatmaps to adversarial attacks. The geometric analysis suggests a fundamental link between the fragility of DNNs against ad-

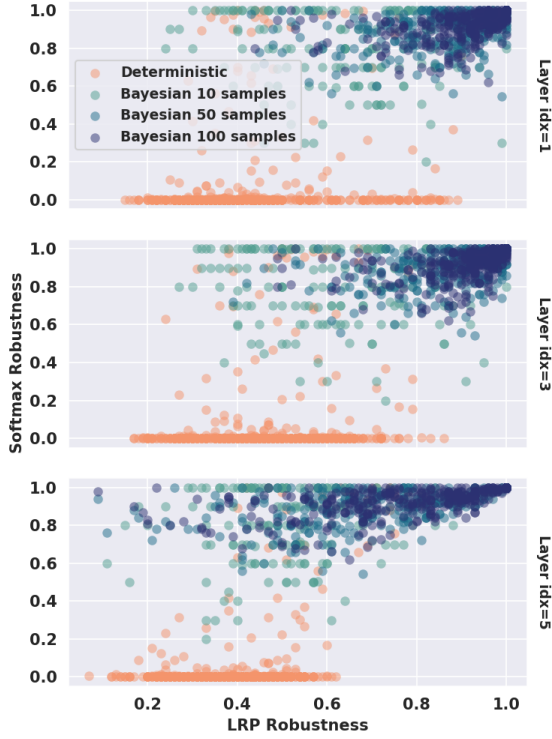


Figure 9: LRP vs Softmax Robustness of deterministic and Bayesian NNs trained on MNIST dataset. LRP Robustness is computed on the 100 most relevant pixels, i.e. using Top₁₀₀. Bayesian Networks are trained with HMC and tested on an increasing number of samples (10, 50, 100). Layer indexes refer to the learnable layers in the architecture (Tab. 2 in the Appendix), which is shared across all models.

versarial attacks and the difficulties in understanding their predictions: because of the unconstrained nature of classifiers defined on high dimensional input spaces but trained on low dimensional data, gradients of both the loss function and the prediction function tend to be dominated by directions which are orthogonal to the data manifold. These directions both give rise to adversarial attacks, and provide spurious explanations which are orthogonal to the natural parametrisation of the data manifold. As shown in Carbone et al. [2020], a Bayesian treatment should, in the limit of infinite data, remedy the situation by averaging out irrelevant gradient directions in expectation. Our empirical findings suggest that the predictions of the infinite data limit seem to hold reasonably well on real data sets: not only BNN interpretations are considerably more robust than deterministic DNN, but we also observe a correlation between softmax (adversarial) robustness and LRP robustness which suggests that indeed Bayesian interpretations capture relevant parametrisations of the data manifold.

While promising, these results are to some extent preliminary: more thorough testing against different adversarial

strategies and different perturbations is certainly warranted. Nevertheless, we believe that the insights provided by a geometric interpretations will be helpful towards a better understanding of both the strengths and the weaknesses of deep learning.

References

David Alvarez-Melis and Tommi S Jaakkola. Towards robust interpretability with self-explaining neural networks. *arXiv preprint arXiv:1806.07538*, 2018.

Sebastian Bach, Alexander Binder, Grégoire Montavon, Frederick Klauschen, Klaus-Robert Müller, and Wojciech Samek. On pixel-wise explanations for non-linear classifier decisions by layer-wise relevance propagation. *PloS one*, 10(7):e0130140, 2015.

Kirill Bykov, Marina M-C Höhne, Klaus-Robert Müller, Shinichi Nakajima, and Marius Kloft. How much can i trust you?—quantifying uncertainties in explaining neural networks. *arXiv preprint arXiv:2006.09000*, 2020.

Ginevra Carbone, Matthew Wicker, Luca Laurenti, Andrea Patane', Luca Bortolussi, and Guido Sanguinetti. Robustness of bayesian neural networks to gradient-based attacks. In H. Larochelle, M. Ranzato, R. Hadsell, M. F. Balcan, and H. Lin, editors, *Advances in Neural Information Processing Systems*, volume 33, pages 15602–15613. Curran Associates, Inc., 2020. URL <https://proceedings.neurips.cc/paper/2020/file/b3f61131b6eceeb2b14835fa648a48ff-Paper.pdf>.

J. Deng, W. Dong, R. Socher, L.-J. Li, K. Li, and L. Fei-Fei. ImageNet: A Large-Scale Hierarchical Image Database. In *CVPR09*, 2009.

Simon Du, Jason Lee, Haochuan Li, Liwei Wang, and Xiyu Zhai. Gradient descent finds global minima of deep neural networks. In *International Conference on Machine Learning*, pages 1675–1685. PMLR, 2019.

Yarin Gal and Zoubin Ghahramani. Dropout as a bayesian approximation: Representing model uncertainty in deep learning. In *international conference on machine learning*, pages 1050–1059. PMLR, 2016.

Amirata Ghorbani, Abubakar Abid, and James Zou. Interpretation of neural networks is fragile. In *Proceedings of the AAAI Conference on Artificial Intelligence*, volume 33, pages 3681–3688, 2019.

Ian Goodfellow, Jonathon Shlens, and Christian Szegedy. Explaining and harnessing adversarial examples. *International Conference on Learning Representations*, 2015. URL <http://arxiv.org/abs/1412.6572>.

Pieter-Jan Kindermans, Sara Hooker, Julius Adebayo, Maximilian Alber, Kristof T Schütt, Sven Dähne, Dumitru Erhan, and Been Kim. The (un) reliability of saliency methods. In *Explainable AI: Interpreting, Explaining and Visualizing Deep Learning*, pages 267–280. Springer, 2019.

Alex Krizhevsky, Vinod Nair, and Geoffrey Hinton. Cifar-10 (canadian institute for advanced research). URL <http://www.cs.toronto.edu/~kriz/cifar.html>.

Alexey Kurakin, Ian J. Goodfellow, and Samy Bengio. Adversarial examples in the physical world. *CoRR*, abs/1607.02533, 2016. URL <http://arxiv.org/abs/1607.02533>.

Yann LeCun and Corinna Cortes. MNIST handwritten digit database. 2010. URL <http://yann.lecun.com/exdb/mnist/>.

Song Mei, Andrea Montanari, and Phan-Minh Nguyen. A mean field view of the landscape of two-layer neural networks. *Proceedings of the National Academy of Sciences*, 115(33):E7665–E7671, 2018.

Grégoire Montavon, Sebastian Lapuschkin, Alexander Binder, Wojciech Samek, and Klaus-Robert Müller. Explaining nonlinear classification decisions with deep taylor decomposition. *Pattern Recognition*, 65:211–222, 2017.

Grégoire Montavon, Alexander Binder, Sebastian Lapuschkin, Wojciech Samek, and Klaus-Robert Müller. Layer-wise relevance propagation: an overview. *Explainable AI: interpreting, explaining and visualizing deep learning*, pages 193–209, 2019.

Radford M Neal et al. Mcmc using hamiltonian dynamics. *Handbook of markov chain monte carlo*, 2(11):2, 2011.

Grant M Rotskoff and Eric Vanden-Eijnden. Neural networks as interacting particle systems: Asymptotic convexity of the loss landscape and universal scaling of the approximation error. *stat*, 1050:22, 2018.

Martin J Wainwright and Michael Irwin Jordan. *Graphical models, exponential families, and variational inference*. Now Publishers Inc, 2008.

Han Xiao, Kashif Rasul, and Roland Vollgraf. Fashion-mnist: a novel image dataset for benchmarking machine learning algorithms. *arXiv preprint arXiv:1708.07747*, 2017.

Xinyang Zhang, Ningfei Wang, Hua Shen, Shouling Ji, Xiapu Luo, and Ting Wang. Interpretable deep learning under fire. In *29th {USENIX} Security Symposium ({USENIX} Security 20)*, 2020.

6 APPENDIX

6.1 LEARNABLE LAYERS

Learnable layers in conv. architecture		
Idx	Layer	Parameters
0	2D Convolution	in_channels = 784 out_channels = 16 kernel_size = 5
3	2D Convolution	in_channels = 16 out_channels = hidden size kernel_size = 5
7	Fully connected	out_features = 10

Table 1: Learnable layers and corresponding indexes in the convolutional architecture. Hidden size equals 512 for models trained on MNIST and 1024 for models trained on Fashion MNIST.

Learnable layers in f.c. architecture		
Idx	Layer	Parameters
1	Fully connected	in_features = 784 out_features = hidden size
3	Fully connected	in_features = hidden size out_features = hidden size
5	Fully connected	in_features = hidden size out_features = 10

Table 2: Learnable layers and corresponding indexes in the fully connected architecture. Hidden size equals 512 for models trained on MNIST and 1024 for models trained on Fashion MNIST.